



Deposited via The University of York.

White Rose Research Online URL for this paper:

<https://eprints.whiterose.ac.uk/id/eprint/95047/>

Version: Published Version

Article:

Booth, N., Robinson, A. P L, Hakel, P. et al. (2015) Laboratory measurements of resistivity in warm dense plasmas relevant to the microphysics of brown dwarfs. Nature Communications. 8742. ISSN: 2041-1723

<https://doi.org/10.1038/ncomms9742>

Reuse

Items deposited in White Rose Research Online are protected by copyright, with all rights reserved unless indicated otherwise. They may be downloaded and/or printed for private study, or other acts as permitted by national copyright laws. The publisher or other rights holders may allow further reproduction and re-use of the full text version. This is indicated by the licence information on the White Rose Research Online record for the item.

Takedown

If you consider content in White Rose Research Online to be in breach of UK law, please notify us by emailing eprints@whiterose.ac.uk including the URL of the record and the reason for the withdrawal request.

ARTICLE

Received 13 May 2014 | Accepted 28 Sep 2015 | Published 6 Nov 2015

DOI: 10.1038/ncomms9742

OPEN

Laboratory measurements of resistivity in warm dense plasmas relevant to the microphysics of brown dwarfs

N. Booth¹, A.P.L. Robinson¹, P. Hake^{2,†}, R.J. Clarke¹, R.J. Dance³, D. Doria⁴, L.A. Gizzi⁵, G. Gregori⁶, P. Koester⁵, L. Labate⁵, T. Levato^{5,†}, B. Li¹, M. Makita⁴, R.C. Mancini², J. Pasley^{1,3}, P.P. Rajeev¹, D. Riley⁴, E. Wagenaars³, J.N. Waugh³ & N.C. Woolsey³

Since the observation of the first brown dwarf in 1995, numerous studies have led to a better understanding of the structures of these objects. Here we present a method for studying material resistivity in warm dense plasmas in the laboratory, which we relate to the microphysics of brown dwarfs through viscosity and electron collisions. Here we use X-ray polarimetry to determine the resistivity of a sulphur-doped plastic target heated to Brown Dwarf conditions by an ultra-intense laser. The resistivity is determined by matching the plasma physics model to the atomic physics calculations of the measured large, positive, polarization. The inferred resistivity is larger than predicted using standard resistivity models, suggesting that these commonly used models will not adequately describe the resistivity of warm dense plasma related to the viscosity of brown dwarfs.

¹Central Laser Facility, STFC Rutherford Appleton Laboratory, Didcot OX11 0QX, UK. ²Department of Physics, College of Science, University of Nevada, Reno, Nevada 89557-0208, USA. ³Department of Physics, York Plasma Institute, University of York, Heslington York YO10 5DD, UK. ⁴School of Mathematics and Physics, Queen's University Belfast, Belfast BT1 4NN, UK. ⁵Intense Laser Irradiation Laboratory, Istituto Nazionale di Ottica, Area della Ricerca del CNR, 56124 Pisa, Italy. ⁶Department of Physics, University of Oxford, Oxford OX4 3PU, UK. † Present addresses: Division of Computational Physics, Los Alamos National Laboratory, Los Alamos, New Mexico 87545, USA (P.H.); ELI Beamlines, Fyzikalni Ustav AV CR Vvi, 182 21 Prague, Czech Republic (T.L.). Correspondence and requests for materials should be addressed to N.B. (email: nicola.booth@stfc.ac.uk) or to N.C.W. (email: nigel.woolsey@york.ac.uk).

Intense laser interactions with matter provide us with the ability to probe the conditions present at the core of dense stars in the laboratory¹. Brown dwarfs are an ideal candidate for study with laboratory plasmas as their cores are at temperatures and mass densities of $\sim 2\text{--}3 \times 10^6 \text{ K}$ ($\sim 200 \text{ eV}$) and $10^2\text{--}10^3 \text{ g cm}^{-3}$, respectively², which are comparable to conditions in laser-produced plasmas. The viscosity and equation of state of these systems are uncertain and requires detailed modelling³. The heat transport and electron propagation models at high density and pressure are complex^{4–7} and need benchmarking. Laser-produced plasmas are a method of creating matter at conditions that approach those believed to occur in brown dwarfs^{8,9} enabling laboratory studies of the plasma in these systems¹⁰.

Plasma polarization spectroscopy is an *in-situ* method for probing the resistivity inside warm dense plasma environments^{11–13}. The technique is sensitive to the complex electron microphysics of collisions in a solid, allowing us to observe the non-equilibrium states in the electron distributions. Other measurements have provided an indirect method of examining the sensitivity of electron transport to low-temperature resistivity in thick, cold, targets (for example, refs 14–19) and electron conductivity models of aluminium have been examined through exploding wire experiments to determine the expansion rate through X-ray backlighter radiographs²⁰. As the resistivity of a laboratory plasma and the viscosity of the plasma of a brown dwarf are both dependent upon electron collisions²¹ and the Coulomb logarithm, $\ln A$, examining the resistivity models in laser-produced plasmas allows us to provide tests of the viscosity of matter found in brown dwarfs, which can be considered to be in local thermodynamic equilibrium. The laboratory measurements of return current distributions are characterized by a Maxwellian distribution of isotropic equilibrium (f_M), which gives these measurements relevance to local thermodynamic equilibrium conditions, and a beam component, which is a small perturbation from the isotropic equilibrium distribution (f_b), given by $f = f_M + f_b \cos\theta$.

In the case of brown dwarfs, the diffusion coefficient is inversely proportional to the viscosity, and as such any changes in the understanding of the viscosity model will therefore influence the temperatures of the brown dwarf. The temperature has an effect on the timescale and mixing in the radiative part of the atmosphere^{22–25}, affecting the brown dwarf evolutionary models. As both systems are dependent on the Coulomb logarithm, a laboratory measurement of the resistivity would therefore constrain the viscosity in a brown dwarf.

In ultra-intense laser-plasma interactions, beams of relativistic ‘hot’ electrons are driven from the interaction region⁶ into materials of much higher density. Anisotropies in the speed distributions of both hot and return currents generate polarized X-ray line emission. As such the experimental measurements of the degree of polarization give us a unique ability to model both the non-equilibrium anisotropy in the return current electron distribution function^{12,13,26} and in turn allows us to evaluate the resistivity generated in the warm dense matter regime applicable to the study of the viscosity of brown dwarfs. It is the non-equilibrium, or anisotropic, parts of the return current distribution that yield information about material resistivity. The return current density J_{rc} is related to the resistivity, η , by the resistive electric field $E = -\eta J_{rc}$, which converts the energy of the hot electrons into Ohmic heating^{16,27}. We can infer the resistivity from electron beam anisotropy, as the fast electrons are generated with an anisotropic distribution function, and this is enhanced by their propagation into the target¹⁶.

Here we demonstrate experimental measurements of the polarization of X-rays produced in intense laser-plasma

interactions as a method of determining resistivity models in warm dense matter. Through doping a low-atomic number (plastic) foil target with sulphur and observing the polarization of emitted X-rays, we observe anisotropic current distributions that drive the heat transport. Our experimental measurements show a high, positive, X-ray polarization arising from anisotropic electron transport. By matching the measured polarization to detailed modelling we show that the commonly used resistivity models do not adequately describe these amorphous materials.

Results

Experimental set-up. Our experiment was performed using the Vulcan Petawatt laser at the Central Laser Facility; with on target intensities of $\sim 5 \times 10^{20} \text{ W cm}^{-2}$ with sulphur-doped plastic targets (polysulphone, $\text{C}_{27}\text{H}_{26}\text{O}_6\text{S}$; for the full description of the experimental set-up, including laser parameters and diagnostics, see Fig. 1 and Methods section). The measurements were performed with an orthogonal pair of highly oriented pyrolytic graphite (HOPG) crystals at a Bragg angle, $\vartheta_B = 45^\circ$ (where the intensity of the *p*-polarized reflection is given by $I_p \approx R(\theta)\cos^2(2\vartheta_B)$), which allows us to observe time-integrated measurements of both polarizations of emitted X-rays in a single shot. The degree of polarization of X-rays emitted is calculated by $P = \frac{I_x - I_y}{I_x + I_y}$ (ref. 11), and the sign of the polarization indicates whether it arises due to beam-directional electrons with energies close to or far exceeding the excitation potential. We define a quantization axis as the direction of the free electron current. When a free electron with energy close to the excitation potential excites a ground state atomic electron, the atomic electron oscillates mostly parallel to the quantization axis. As a result, the atomic electron selects certain excited states emitting π -polarized dipole radiation (that is, $P > 0$) as it de-excites. In contrast, an energetic free electron will exert a pulse of electric field that is perpendicular to the quantization axis causing the atomic electron to oscillate and emit mostly σ -polarized radiation (that is, $P < 0$).

Experimental polarization measurements. The degree of polarization in the Ly- α transitions of sulphur, obtained from the data shown in Fig. 2, was measured to be $P = +0.16 \pm 0.04$. This value for the polarization indicates a beam of free electrons in the

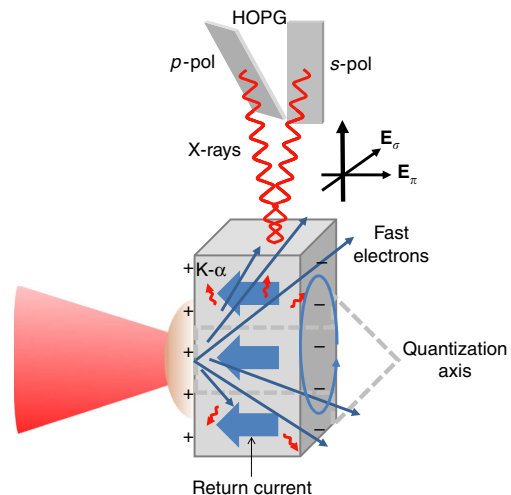


Figure 1 | The generation of polarized X-rays in a laser-plasma interaction. The target geometry of a high-intensity pulse, incident on a foil target produces polarized X-rays. These polarized X-rays are recorded by the orthogonal pair of HOPG crystals positioned above the target (not to scale) to measure each polarization independently in a single shot.

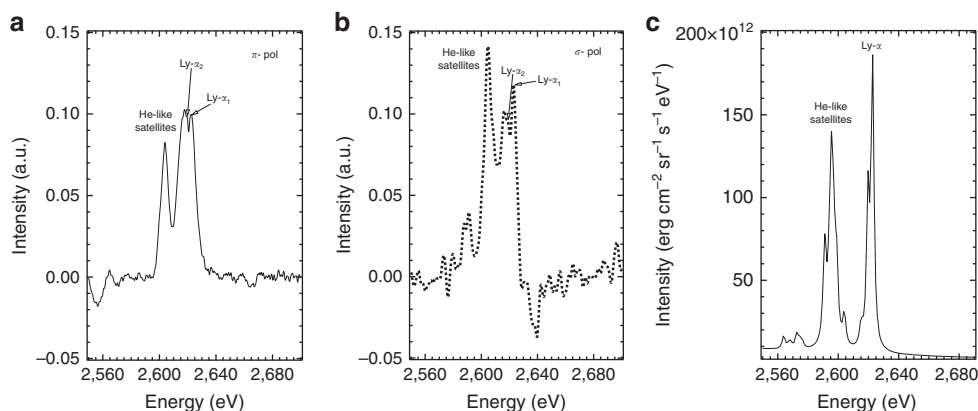


Figure 2 | X-ray spectrum from a 25- μm -thickness sulphur-doped plastic (polysulphone) target. The two plots show the (a) π -polarized X-ray (—) and (b) σ -polarized X-ray (.....) spectrum from the same shot. The degree of polarization observed in the He- α lines differ from those of the Ly- α , as these lines are a result of interplay between direct collisional excitation within the He-like ion as well as electron capture from the ground state²⁹ and provide a future avenue for study. The third plot (c) is the simulated emission spectra of polysulphone modelled using the collisional-radiative spectral analysis code PrismSPECT³⁷ with a temperature of $T_b = 150$ eV and $\alpha = 0.01$.

return current close to the excitation potential (≥ 2.8 keV). This has led us to use the non-equilibrium, anisotropic, velocity distribution of the return current to explore the resistivity in warm dense plasmas. The experimental measurement of the polarization is time-integrated, and whilst laboratory plasmas do change on very fast timescales, it does not prevent a comparison with theoretical models. Uncertainties in the measurement are discussed in the Methods section.

Simulations of the electron transport and polarization. These measurements are modelled using the ZEPHYROS²⁸ and POLAR²⁹ codes to calculate plasma hybrid electron kinetics and atomic magnetic sub-level population kinetics respectively. POLAR requires three electron populations and temperatures³⁰ to calculate the polarization, and so by varying the input to ZEPHYROS to give us values for background temperature T_b , return current temperature T_{rc} and hot electron fraction α , we can iterate between the two codes to find the conditions that most closely match the experimental observations. Using this process we find that there is a balance to be achieved between T_b , T_{rc} and α that maximizes the degree of polarization. If T_b is too high, the depolarizing Maxwellian electrons will equilibrate P towards zero and equally, if T_{rc} is too low, the beam is ineffective in driving anisotropy.

On taking some typical values from ZEPHYROS: $T_b = 200$ eV, $T_{rc} = 600$ eV and hot temperature $T_h = 7$ MeV (from Wilks' scaling³¹) with $\alpha = 0.0032$, we obtain a polarization value from the POLAR model of $P = +0.14$. The bulk temperature T_b is in the typical temperature region in the core of brown dwarfs. The ZEPHYROS simulations using the above electron distribution parameters are shown in Fig. 3. In the region shown, heating is dominated by resistive heating of the target by the anisotropic component of the return current.

To compare this model combination to the experimental results we carried out temporal and spatial averaging of the post-processed ZEPHYROS output. Two resistivity models were compared: the Lee-More⁵ model, and the Spitzer⁴ model (with an initial temperature of 50 eV). These two resistivity models primarily differ at low temperatures, where the Spitzer resistivity curve is significantly higher. The simulation results for the different resistivity models are shown in Fig. 4. The figures show the plasma material with the region with the strongest Ly- α emission at 2.6 keV highlighted, which arises from a region in the

bulk plasma heated to approximately $T_b = 200$ eV. These plots of background electron temperature show that the target is heated to higher average temperature in the case where the Spitzer resistivity curve was employed compared with that where the Lee-More resistivity curve was used. When these results are processed with POLAR we obtained an average polarization of $P = +0.275 \pm 0.1$ for the Lee-More case and $P = +0.163 \pm 0.03$ for the Spitzer case ($T_{\text{init}} = 50$ eV). This indicates that a model with somewhat higher resistivity at low temperatures than predicted by the Lee-More model is necessary for there to be good quantitative agreement with the experimental results. The simulated polarization is sensitive to T_b for both the Lee-More and the Spitzer ($T_{\text{init}} = 50$ eV) models. For our simulations we use the Wilks scaling which gives $T_h = 7$ MeV, rather than the scaling laws of Beg³², Haines³³ or Sherlock³⁴ which predict lower temperatures. The calculations show Lee-More over predicts the polarization, whilst Spitzer is more consistent with our experimental result. How the polarization calculation varies with T_b for these two models are shown in Supplementary Table 1 and discussed in Supplementary Note 1. These results clearly show that conclusions of this work are not dependent on the T_h model or scaling law. Indeed a factor of >2 reduction in T_h is needed for the Lee-More model to match observation. This reduction cannot be justified using accepted scaling laws.

Discussion

Resistivity models with a low-temperature (< 100 eV) resistivity equal to or lower than the standard Lee-More model with a minimum electron scattering mean free path of $2 \times r_s$ do not agree well with our experimental results. To be clear: our analysis is not suggesting that the Spitzer model is a 'good' model of these plasmas. Rather it suggests that accurate computation of the resistivity at low-temperature (< 100 eV) requires careful examination.

Measuring the polarization state of X-rays to give *in-situ* information about return current electron transport in warm dense matter shows a large degree of anisotropy in the return current distributions. The use of our combination of experiment and computational models allows us to observe a beam-like return current, and use this to interrogate resistivity models of warm dense matter, in this case plastic. We find a model which is highly resistive at low temperatures is necessary to obtain the level of polarization that we observe. This indicates that the

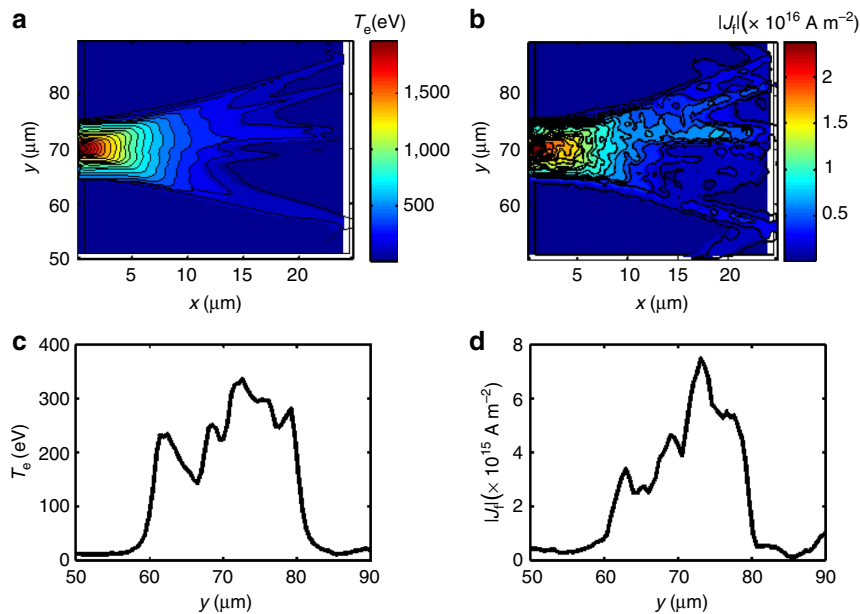


Figure 3 | ZEPHYROS simulations of the sulphur-doped plastic target conditions. The simulations use a combination of plasma hybrid electron kinetics and atomic magnetic sub-level population kinetics to obtain the plasma parameters $T_b = 200$ eV, $T_{rc} = 600$ eV and $\alpha = 0.0032$. The simulation results show the simulated electron temperature (a) and current density (b) and are taken in the mid-plane of the interaction, with x and y the horizontal and vertical axes through the target respectively, and lineouts of each distribution are shown below the simulation taken through middle of the target at $x = 12.5 \mu\text{m}$ (c and d respectively). The parameters selected for the hot electron beam match the experiment and initially use the resistivity model of Davies³⁶.

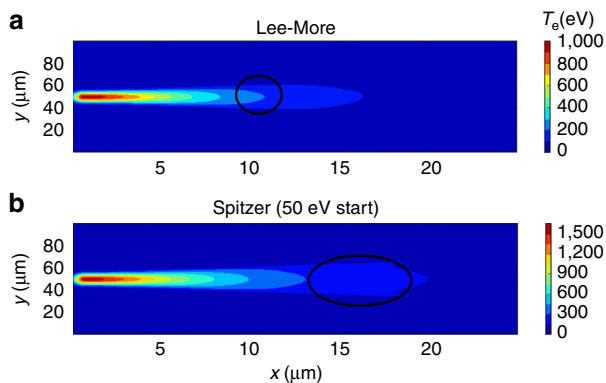


Figure 4 | Simulations comparing the electron temperature profiles. The simulations show the plasma conditions for plasma parameters $T_b = 200$ eV, $T_{rc} = 600$ eV and $\alpha = 0.0032$. The simulation results are again taken in the mid-plane of the interaction, with x and y the horizontal and vertical axes through the target respectively. (a) shows the expected temperature profile with the commonly used Lee-More model starting with a minimum mean free path of $2 \times r_s$. This resistivity condition produces a small volumetric region heated to 200 eV and leads to a calculated polarization of $P = +0.275 \pm 0.1$ (s.d.). Whilst it is possible that the observed polarizations are produced in this small region, the simulation from the Spitzer model with a 50 eV starting temperature in the case shown in b has a much larger region heated to 200 eV, which dominates over any other single temperature region, leading to a calculated polarization of $P = +0.163 \pm 0.03$ (s.d.). In both figures the region heated to 200 eV is highlighted, demonstrating that the region heated to the necessary temperature to generate the observed polarization is larger in the case of the higher resistivity Spitzer model.

resistivity in warm dense plasmas is higher than one would determine from commonly used models, and needs much more careful consideration. Since our resistivity models have to be

significantly altered to understand the energy transport through plasmas, it is likely that the viscosity of the brown dwarf would also need to be modified, potentially leading to a change in temperature which would alter the evolutionary models and luminosity of these objects. With further study, through examining the resistivity of plasmas in the laboratory, it is possible to quantify the coulomb logarithm for brown dwarfs. The modelling of warm dense matter resistivity, and viscosity in the case of brown dwarfs, is so complex, it is clearly necessary to consider in more detail the resistivity curves used in such modelling.

Methods

Laser-target interaction. The experiment was performed with the Vulcan Petawatt system at the Central Laser Facility, Rutherford Appleton Laboratory. The laser pulses contained ~ 250 J in 600 fs on target, at 1,053 nm. The beam is focussed with an $f/3$ parabola and focuses to a best spot of $\approx 6 \times 6 \mu\text{m}^2$ with $\sim 30\%$ of the total energy in the full width at half maximum, with peak intensities of $5 \times 10^{20} \text{W cm}^{-2}$. The nanosecond amplified spontaneous emission contrast ratio was measured on each shot with a fast photodiode at 10^{-6} .

Targets. The targets were 25- μm -thick polysulphone foils ($\text{C}_{27}\text{H}_{26}\text{O}_6\text{S}$) cut to $100 \times 100 \mu\text{m}^2$ squares mounted on copper stalks.

X-ray polarization spectrometer. Two flat, mosaic, $25 \times 50 \times 2 \text{mm}^3$, grade ZYA (mosaic spread $0.4^\circ \pm 0.1^\circ$) HOPG (002) Bragg reflecting crystals were placed above the target aligned either parallel or perpendicular to the target surface, perpendicular to the general direction of hot electrons (the quantization axis). Diffracted X-rays (with $\theta_B \sim 45^\circ$) were recorded on image plates. The use of two high-reflectivity HOPG crystals was essential to enable single-shot spectroscopy measurements in an environment of high-level electromagnetic and particle noise, with relatively weak X-ray signal. (The reflectivity and rocking curves of the HOPG crystals in this context are discussed further in ref. 35).

Experimental degree of polarization. The degree of polarization is extracted by comparing $\text{Ly-}\alpha_1$ integrated line intensities from the orthogonal HOPGs. To unfold the relative contributions of the $\text{Ly-}\alpha$ components and assess the level of uncertainty, a multi-line fitting procedure is applied. This procedure enables a cross calibration of the HOPG spectra by normalizing the integrated intensity of the $\text{Ly-}\alpha_2$ and then extracting the relative integrated intensities of the $\text{Ly-}\alpha_1$ emission. Sources of error

and uncertainty in instrumentation and analysis are scrutinized. The experimental environment is noisy and given the crystals are positioned next to each other above the target and orientated to diffract in different directions the image plates are exposed to different levels of background. This is accounted for in the data analysis as are the uncertainty that arises from the differences in positioning.

Numerical modelling. The plasma electron kinetics simulations have been carried out using the three-dimensional particle hybrid code ZEPHYROS²⁸. The Lyman- α sub-level population calculations were performed with the POLAR²⁹ model, which is a sub-level population, zero-dimensional atomic kinetics code. Hybrid simulations treat the hot electrons kinetically, but the background plasma is treated as a fluid. The parameters selected for the hot electron beam match the experiment and use the resistivity model of Davies' heuristic curve for CH (ref. 36), and modified to give the Spitzer resistivity for sulphur or nickel in the high-temperature limit. From this we extract spatial profiles of the hot electron current density and the 'average' background temperature and density (T_b and n_b), which are used as input to POLAR to calculate the polarization. POLAR includes background electrons as an isotropic Maxwellian population and a return current as a beamed electron population with a longitudinal temperature ($T_{r,c}$) and density zn_b , where α is the return current fraction.

Errors in the calculated polarizations were calculated by performing a study varying the simulation inputs; intensity, pulse duration and absorption. These parameters were varied between upper and lower limits of possible experimental values, to find the likelihood of errors between the experimental data and our simulated polarizations.

References

- Chabrier, G. & Baraffe, I. Theory of low-mass stars and substellar objects. *Ann. Rev. Astron. Astrophys.* **38**, 337–377 (2000).
- Ichimaru, S. & Kitamura, H. Pyonuclear reactions in dense astrophysical and fusion plasmas. *Phys. Plasmas* **6**, 2649–2671 (1999).
- Baraffe, I., Chabrier, G. & Barman, T. The physical properties of extra-solar planets. *Rep. Prog. Phys.* **73**, 016901 (2010).
- Spitzer, L. & Harm, R. Transport phenomena in a completely ionized gas. *Phys. Rev.* **89**, 977–981 (1953).
- Lee, Y. T. & More, R. M. An electron conductivity model for dense plasmas. *Phys. Fluids* **27**, 1273–1286 (1984).
- Bell, A. R., Davies, J. R., Guerin, S. & Ruhl, H. Fast electron transport in high-intensity, short-pulse laser-solid experiments. *Plasma Phys. Control. Fusion* **39**, 653–659 (1997).
- Evans, R. G. Modelling electron transport for fast ignition. *Plasma Phys. Control. Fusion* **49**, B87–B93 (2007).
- Burrows, A. & Liebert, J. The science of brown dwarfs. *Rev. Mod. Phys.* **65**, 301–336 (1993).
- Saumon, D., Chabrier, G. & Van Horn, H. M. An equation of state for low-mass stars and giant planets. *Astrophys. J. Suppl.* **99**, 713–741 (1995).
- Remington, B. A., Arnett, D., Drake, R. P. & Takabe, H. Modelling astrophysical phenomena in the laboratory with intense lasers. *Science* **284**, 1488–1493 (1999).
- Kieffer, J. C. *et al.* Electron distribution anisotropy in laser-produced plasmas from x-ray line polarization measurements. *Phys. Rev. Lett.* **68**, 480–483 (1992).
- Inubushi, Y. *et al.* X-ray line polarization spectroscopy to study hot electron transport in ultra-short laser produced plasma. *J. Quant. Spectrosc. Radiat. Transf.* **99**, 305–313 (2006).
- Kawamura, T. *et al.* Polarization of He- α radiation due to anisotropy in fast electron transport in ultra-intense laser-produced plasmas. *Phys. Rev. Lett.* **99**, 115003 (2007).
- Milchberg, H. M., Freeman, R. R. & Davey, S. C. Resistivity of a simple metal from room temperature to 10⁶ K. *Phys. Rev. Lett.* **61**, 2364–2367 (1988).
- Davies, J. R., Bell, A. R. & Tatarakis, M. Magnetic focussing and trapping of high-intensity laser-generated fast electrons at the rear of solid targets. *Phys. Rev. E* **59**, 6032–6036 (1999).
- Bell, A. R. & Kingham, R. J. Resistive collimation of electron beams in laser produced plasmas. *Phys. Rev. Lett.* **91**, 035003 (2003).
- MacLellan, D. A. *et al.* Annular fast electron transport in silicon arising from low-temperature resistivity. *Phys. Rev. Lett.* **111**, 095001 (2013).
- DeSilva, A. W. & Katsouras, J. D. Electrical conductivity of dense copper and aluminum plasmas. *Phys. Rev. E* **57**, 5945–5951 (1998).
- Brown, C. R. D. *et al.* Measurements of electron transport in foils irradiated with a picosecond timescale laser pulse. *Phys. Rev. Lett.* **106**, 185003 (2011).
- Sinars, D. B. *et al.* Exploding aluminium wire expansion rate with 1–4.5kA per wire. *Phys. Plasmas* **7**, 1555–1563 (2000).
- Mohanty, S. *et al.* Activity in very cool stars: Magnetic dissipation in late M and L dwarf atmospheres. *Astrophys. J.* **571**, 469–486 (2002).
- Saumon, D. *et al.* Physical parameters of very cool T dwarfs. *Astrophys. J.* **656**, 1136–1149 (2007).
- Leggett, S. K. *et al.* The physical properties of four \sim 600K T dwarfs. *Astrophys. J.* **695**, 1517–1526 (2009).
- Stephens, D. C. *et al.* The 0.8 – 14.5 μ m spectra of mid-L to mid-T dwarfs: diagnostics of effective temperature, grain sedimentation, gas transport and surface gravity. *Astrophys. J.* **702**, 154–170 (2009).
- Leggett, S. K. *et al.* Properties of the T8.5 dwarf wolf 940B. *Astrophys. J.* **720**, 252–258 (2010).
- Inubushi, Y. *et al.* Analysis of x-ray polarization to determine three-dimensionally anisotropic velocity distributions of hot electrons in plasma produced by ultrahigh intensity lasers. *Phys. Rev. E* **75**, 026401 (2007).
- Huang, X. & Cumming, A. Ohmic dissipation in the interiors of hot Jupiters. *Astrophys. J.* **757**, 47 (2012).
- Kar, S. *et al.* Guiding of relativistic electron beams in solid targets by resistively controlled magnetic fields. *Phys. Rev. Lett.* **102**, 055001 (2009).
- Hakel, P. & Mancini, R. C. X-ray line polarization of He-like Si satellite spectra in plasmas driven by high-intensity ultrashort pulsed lasers. *Phys. Rev. E* **69**, 056405 (2004).
- Hakel, P. Polarization properties of the Ly- α line from sulphur plasmas driven by high-intensity, ultrashort-duration laser pulses. *Can. J. Phys.* **89**, 509–511 (2011).
- Wilks, S. C. & Kruer, W. L. Absorption of ultrashort, ultra-intense laser light by solids and overdense plasmas. *IEEE J. Quantum Electron.* **33**, 1954–1968 (1997).
- Beg, F. N. *et al.* A study of picosecond laser–solid interactions up to 1×10^{19} W cm⁻². *Phys. Plasmas* **4**, 447–457 (1997).
- Haines, M. G. *et al.* Hot-electron temperature and laser-light absorption in fast ignition. *Phys. Rev. Lett.* **102**, 045008 (2009).
- Sherlock, M. Universal scaling of the electron distribution function in one-dimensional simulations of relativistic laser-plasma interactions. *Phys. Plasmas* **16**, 103101 (2009).
- Woolsey, N. C. *et al.* Precision x-ray spectroscopy of intense laser-plasma interactions. *High Energy Density Phys.* **7**, 105–109 (2011).
- Davies, J. R. How wrong is collisional Monte Carlo modelling of fast electron transport in high-intensity, laser-solid interactions? *Phys. Rev. E* **65**, 026407 (2002).
- McFarlane, J. J. *et al.* Simulation of the ionization dynamics of aluminum irradiated by intense short-pulse lasers. *Proc. Inertial Fusion and Sciences Applications 2003. Amer. Nucl. Soc.* 457–469 (2004).

Acknowledgements

We would like to acknowledge the support and expertise of the staff of the Central Laser Facility. This work was partially supported by the Extreme Light Infrastructure Project, the HiPER project, the United Kingdom Engineering and Physical Sciences Research Council (grant number EP/H012605/1) and the Science and Technology Facilities Council. The work of GG has received partial funding from the European Research Council under the European Community's Seventh Framework Programme (FP7/2007–2013)/ERC grant agreement no. 256973.

Author contributions

The experiment was conceived by N.C.W., G.G. and P.P.R. The experiment, planning and analysis were carried out by N.B. and N.C.W. with contributions from R.J.C., D.D., L.A.G., G.G., P.K., L.L., T.L., B.L., M.M., J.P., P.P.R., D.R., E.W., R.J.D. and J.N.W. Simulations were carried out by A.P.L.R., P.H. and R.C.M., N.B., P.H., A.P.L.R., P.P.R. and N.C.W. prepared the manuscript.

Additional information

Supplementary Information accompanies this paper at <http://www.nature.com/naturecommunications>

Competing financial interests: The authors declare no competing financial interests.

Reprints and permission information is available online at <http://npg.nature.com/reprintsandpermissions/>

How to cite this article: Booth, N. *et al.* Laboratory measurements of resistivity in warm dense plasmas relevant to the microphysics of brown dwarfs. *Nat. Commun.* 6:8742 doi: 10.1038/ncomms9742 (2015).



This work is licensed under a Creative Commons Attribution 4.0 International License. The images or other third party material in this article are included in the article's Creative Commons license, unless indicated otherwise in the credit line; if the material is not included under the Creative Commons license, users will need to obtain permission from the license holder to reproduce the material. To view a copy of this license, visit <http://creativecommons.org/licenses/by/4.0/>